PROCEEDINGS OF SPIE

SPIEDigitalLibrary.org/conference-proceedings-of-spie

Optical design of MAAT: an IFU for the GTC OSIRIS spectrograph

Robert Content, Francisco Prada, Enrique Pérez, Carlos Domínguez-Tagle, Manuela Abril, et al.

Robert Content, Francisco Prada, Enrique Pérez, Carlos Domínguez-Tagle, Manuela Abril, Gabriel Gómez, Kilian Henríquez, Jon Lawrence, Guillermo González de Rivera, Ariel Goobar, Jens Hjorth, M. Ángeles Perez García, Adriano Agnello, David Jones, "Optical design of MAAT: an IFU for the GTC OSIRIS spectrograph," Proc. SPIE 12184, Ground-based and Airborne Instrumentation for Astronomy IX, 1218465 (29 August 2022); doi: 10.1117/12.2630717

SPIE.

Event: SPIE Astronomical Telescopes + Instrumentation, 2022, Montréal, Québec, Canada

Optical Design of MAAT: an IFU for the GTC OSIRIS Spectrograph

Robert Content[a]*, Francisco Prada[b], Enrique Perez[b], Carlos Domínguez-Tagle[b], Manuela Abril[c], Gabriel Gómez[c], Kilian Henríquez[c], Jon Lawrence[a], Guillermo González de Rivera[d], Ariel Goobar[e], Jens Hjorth[f], Ángeles Perez García[g], Adriano Agnello[f], David Jones[h]
[a]Australian Astronomical Optics - Macquarie University, Australia; [b]Instituto de Astrofísica de Andalucía; [c]Gran Telescopio CANARIAS, La Palma, Spain; [d]Escuela Politécnica Superior, Universidad Autónoma de Madrid, Spain; [e]The Oskar Klein Centre, Stockholm University, Sweden; [f]DARK, Niels Bohr Institute, University of Copenhagen, Denmark; [g]Departamento de Física Fundamental, Universidad de Salamanca, Spain; [h]Instituto de Astrofísica de Canarias, Tenerife, Spain

ABSTRACT

The Mirror-slicer Array for Astronomical Transients (MAAT) is a new IFU for the OSIRIS spectrograph on the 10.4-m Gran Telescopio CANARIAS (GTC) at La Palma, spectrograph that has been recently upgraded with a new detector and moved to the Cassegrain focus. Funding has been secured to build MAAT. We present the nearly final design, its expected performances, the different options that were studied, and an analysis of the spectrograph aberrations. MAAT will take advantage of the OSIRIS mask cartridge for multi-object spectroscopy. The IFU will be in a box that will take the place of a few masks. It is based on the Advanced Image Slicer (AIS) concept as are MUSE and KMOS on the VLT (among many others). The field is 10" x 7" with 23 slices 0.305" wide giving a spaxel size of 0.254" x 0.305". The wavelength range is 360 nm to 1000 nm. The small space envelope, the maximum weight of the mask holder, and the curvature and tilt of the slit created additional design challenges. The spectral resolution will be about 1.6 times larger than with a standard slit of 0.6" because of the smaller size of the slices. All the eleven VPHs and grisms will be available to provide a broad spectral coverage with low to intermediate resolution (R=600 to 4100). To maximize the resolution of a spectrograph designed for a slit twice the width of the slices, we are in the process of measuring the wavefront of the spectrograph aberrations by using 2 out-of-focus masks with pinholes along the slit. We will then correct some of these aberrations with MAAT.

Keywords: image slicer, integral field unit, OSIRIS spectrograph, GTC.

1. INTRODUCTION

Integral field spectroscopy is now universally used on large telescopes. The GMOS IFUs [3] on the GMOS spectrographs and NIFS [2] have been in operation on Gemini for a very long time. A good example is the two very powerful integral field spectrographs of the VLT: KMOS [6] and MUSE [1]. While KMOS combines Multi-Object Spectroscopy with Integral Field Spectroscopy with its 24 IFUs, MUSE is the most powerful integral field spectrograph in the world on a fully steerable large telescope. We are now in the process of finalizing the optical design of the Mirror-slicer Array for Astronomical Transients (MAAT), a project of IFU for the OSIRIS spectrograph on GTC. Maat is the Egyptian goddess of cosmic harmony, peace, truth and justice, a well suited companion for the OSIRIS spectrograph. OSIRIS is an imaging and Multi-Object Spectrograph (MOS) using masks. It has a cartridge (also called juke box) with 13 slots, each for a mask. Some masks have a simple slit while others are multi-slit masks. The IFU will be in a box that takes the place of a few masks, probably 6 or 7. The structure of the box will use a standard or reinforced frame normally used to hold a mask. The frame has the correct shape to fit in a slot of the OSIRIS cartridge. The box will be attached to that frame (Figure 1). In the day, the IFU can be inserted or removed and more masks inserted depending of the observations to be done in the next night. The IFU design will follow the concept of Advanced Image Slicer as in MUSE and KMOS on the VLT, and in the NIRSpec and MIRI [14] spectrographs of JWST.

*contentrobert0@gmail.com

Ground-based and Airborne Instrumentation for Astronomy IX, edited by Christopher J. Evans, Julia J. Bryant, Kentaro Motohara, Proc. of SPIE Vol. 12184, 1218465
© 2022 SPIE · 0277-786X · doi: 10.1117/12.2630717

At the slit, 3 different options of optics have been studied because of the challenge created by the unusual characteristics of the slit. Because the telescope has a curved focal plane and the slit centre is very much off-axis with respect to the telescope, the slit is curved and tilted with respect to the direction of the beam. Another challenge is the large maximum incident angle on the reimaging mirror array of the IFU which can generate large aberrations if a standard design is use. The biggest challenge happened to be the maximum weight that the mask holder can sustain. Finally, there is the challenge of having a high IFU transmission for the whole range from 360 nm to 1000 nm while both reflective and anti-reflection coatings do not easily deliver a high efficiency for such a large range and such a blue end. Both reflective and transmissive optics were studied but the transmissive option was abandoned due to the different constraints and its lower performances. The present paper describes the nearly final design of MAAT.

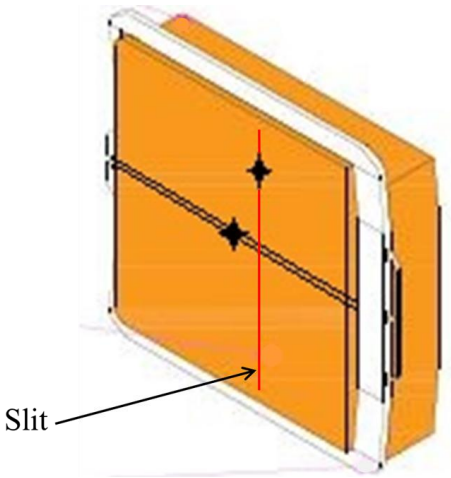

Figure 1. Preliminary mechanical design of the box. The standard mask frame is in white around the box. The apparent horizontal slit is in fact the back-image of the gap between the original two 2k x 4k detectors that have now been replaced by a 4k x 4k with a higher transmission. The top black star is the position of the telescope axis while the bottom is the OSIRIS axis.

MAAT will provide the GTC community with highly competitive unique observing capabilities complementary to the existing instrumentation, i.e. seeing-limited and wide-band IFS at low / moderate spectral resolution, higher than the standard resolution of OSIRIS; all photons are collected, and a larger efficiency is obtained; it can perform absolute spectro-photometry; advantage on bad (any) seeing conditions since MAAT keeps its nominal spectral resolution regardless of the seeing; target acquisition with no overheads.

The science potential of MAAT is essentially unlimited as presented in detail in the White Paper on MAAT [15]. This includes the nature of the diffuse universe (the intergalactic and circumgalactic mediums), strong galaxy lensing studies, time-domain cosmography with strongly lensed quasars and supernovae, identification and characterization of EM-GW counterparts, exploration of the host galaxy environment of supernovae, binary masses and nebulae abundances, brown dwarfs and planetary mass objects, and synergies with worldwide telescopes and other facilities on La Palma. Furthermore, MAAT top-level requirements allow broadening its use to the needs of the GTC community for a wide range of competitive science topics given its unique observing capabilities.

2. OPTICAL DESIGN

The optical design is based on the concept of Advanced Image Slicer [5][10][11] (Figure 2). In the standard design, the focal plane of the telescope is reimaged by fore-optics on an array of long and thin mirrors that slice the field in correspondingly long and thin images. This mirror array is called the slicing mirror, or slicer. The beam from each slice is sent to a mirror that reimages the slice on the slit. A pupil of the telescope is imaged on (or nearby) that reimaging mirror by the slice mirror, so its name of pupil mirror. This permits to avoid vignetting present on previous slicer designs. All slice images are side-by-side on the slit. A final mirror on the slit reimages the pupil at the right place in the spectrograph. Along the length of the slices, the spaxel width is determined by the size of a pixel on the detector in the

spectrograph spatial direction. In the spectral direction, it is the slice width that determines the size of a spaxel. This gives spaxels of 0.254" x 0.305" in the final MAAT design.

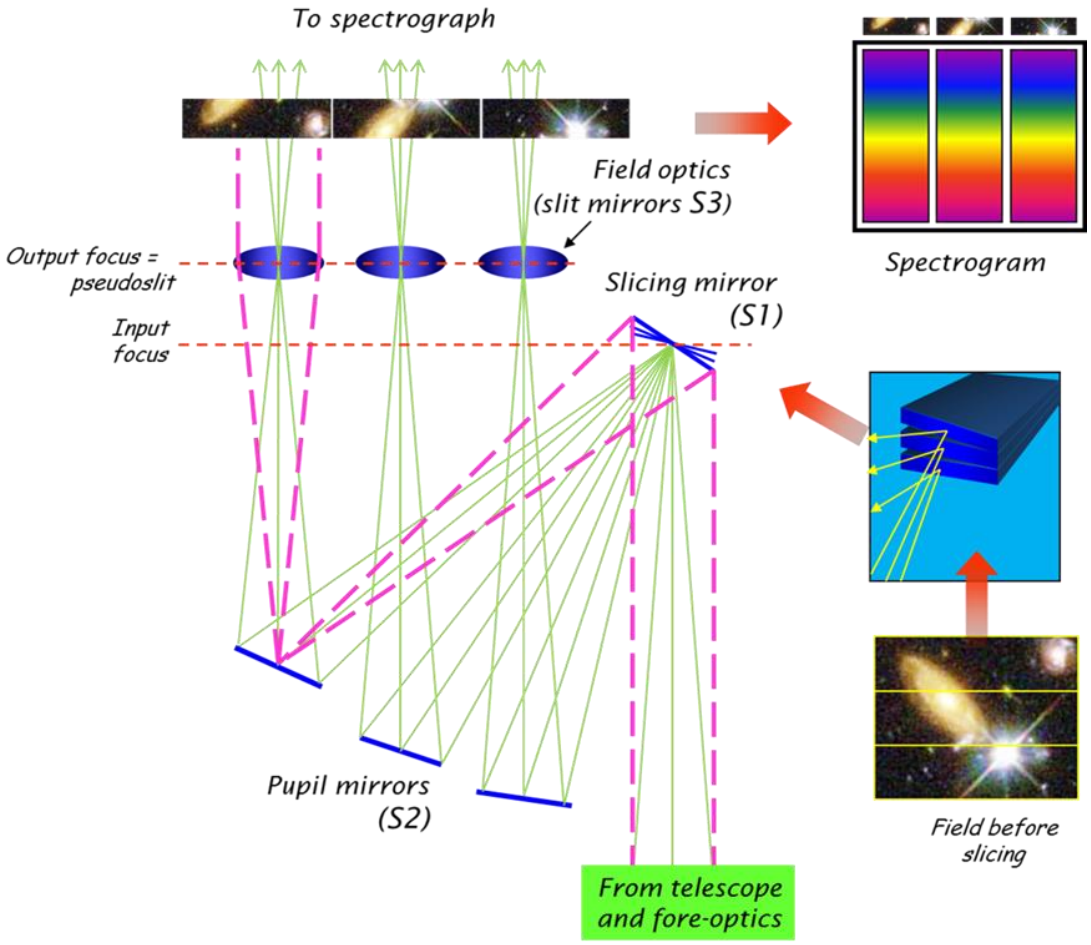

Figure 2. Basic principle of the Advanced Image Slicer.

2.1 Slit mirrors

We studied 3 options of mirrors on the slit. The first option is that of the standard AIS design with one slit mirror for each slice. The second is a modification to the Advanced Image Slicer design that was developed by the then Edinburg Observatory [14]. They reasoned that only 2 mirrors are necessary to reimage the field and the pupil so 2 mirror arrays should be enough, not 3. They then removed the slit mirror array and replaced it by 2 long rectangular mirrors, and modified the curvature of the other optics accordingly. This simplifies the mechanical design and in principle reduces the cost but it brings some problems. First, it degrades the field and pupil image qualities; second, it is impossible to have a unique linear slit, the slit needs to be "staggered." Figure 3 shows the result. Apart from reducing the length of the spectra, it worsens cross-contamination because bright lines as OH lines can contaminate a region of faint lines in an adjacent slice image.

A possibly more important disadvantage that may cancel the cost reduction is that it makes alignment more difficult. Manufacturers have brought this point to us. For MAAT, it is not necessarily a serious problem because we are not working at the near diffraction limit design which asks for particularly high angular precision.

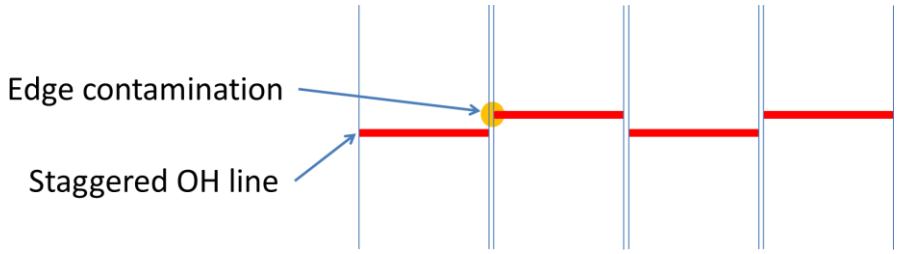

Figure 3. Sketch of the effect of a staggered slit in the version of the AIS developed by the then Edinburg Observatory. It represents the spectra from 4 slices where a bright OH line contaminates adjacent regions where faint object lines can be present.

There is a third option, one that keeps some of the advantages of the Edinburg version of the AIS while removing the staggered slit. There is again a slit mirror array but one that is of much lower cost because it is made of 2 staggered flat mirrors. The staggered slit is then replaced by a linear slit as in the standard design of the AIS. The field and pupil image degradation still remains however as the increased difficulty of doing the alignments. Figure 4 shows a sketch of the design. The 2 staggered mirrors are interleaved to create a simple slit mirror array. Note that there is not much difference between the staggered slit and staggered mirror options from an optical point of view.

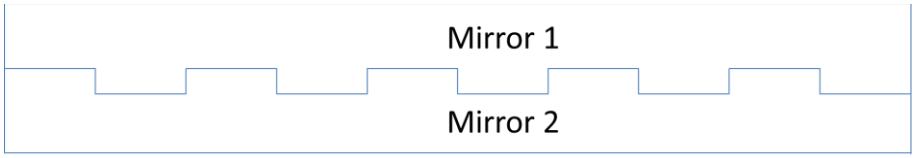

Figure 4. Layout of staggered mirrors creating a slit mirror array.

We studied all 3 options but came back to the standard AIS design mostly because it simplifies the alignment of the pupil position in the spectrograph which has a grating with a very tight aperture. It also gives better as-designed image quality in the focal and pupil planes.

2.2 Field of view

A classic problem with an IFU is its aspect ratio. What value to choose? The very first AIS (on the first GNIRS spectrograph [10]) aspect was chosen using the following reasoning which was determined by the first author for his very first IFU design, a fibre-lenslet IFU for UIRT [16]: A typical astronomical object will have a width and a length, so a square field is not optimum. If the object is too large for the field, a second image will have to be taken. We want the same optimum aspect ratio for the total image obtained by merging these 2 images. Since the ratio is the same for one or 2 merged images, we have:

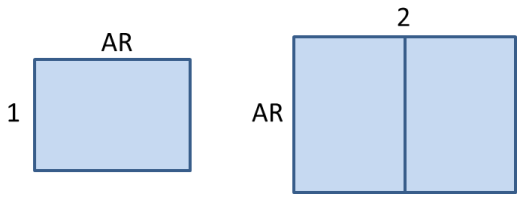

$$AR/1 = 2/AR \rightarrow AR = Sqrt(2)$$

So the optimum aspect ratio is Sqrt(2) but this is a rule of thumb, the aspect ratio only needs to be near that value. Another point is that a larger aspect ratio reduces the number of slices for a fixed surface area which reduces the cost but the PSF will be worse on the slice images because they are longer. Values around 1.3-1.5 are fine.

The field of view of the preliminary concept was based on the maximum slit length possible. It was 14.2" x 10" but a preliminary look at the mechanical design showed that it was too heavy; we then reduced the field to 12" x 8.5". A full mechanical design however showed that this still gives a weight too high for the mask holder. The field had to be reduced again but the mask holder will also be upgraded to limit the reduction. Fortunately, the weight goes down fast with a reduction of the field size. The slit length is about proportional to the field surface area so the optics and their holder goes at least with the power 2 of the size (assuming a fixed aspect ratio). Most of the weight is in the plate holding the optics which weight goes down even faster since it is proportional to a power 2 to 3 of the slit length, so 4 to 6 of the field size. We settled for a field of 10" x 7" and a new reinforced holder to sustain an IFU of 5 kg plus a frame of 2.5 kg.

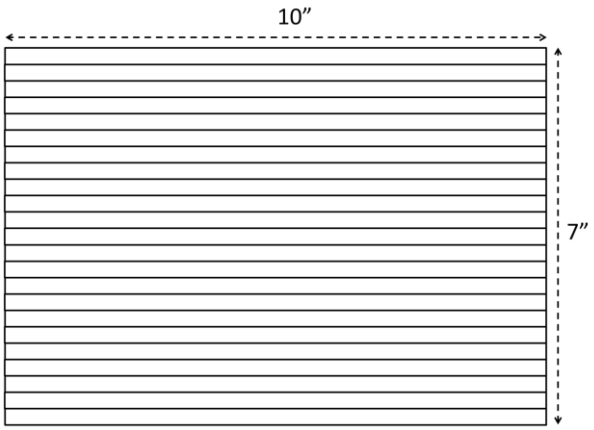

Figure 5. Final size of the field, there are 23 slices.

2.3 Telescope pupil

The pupil of the spectrograph has a complex shape because the primary is a "puzzle" of smaller mirrors as the Keck primary. The secondary is in fact the stop of the telescope but it has the same shape than the primary. This already make the optical design more difficult to optimize but a complication is the derotator that rotates the pupil while observing which slightly changes the PSF shape.

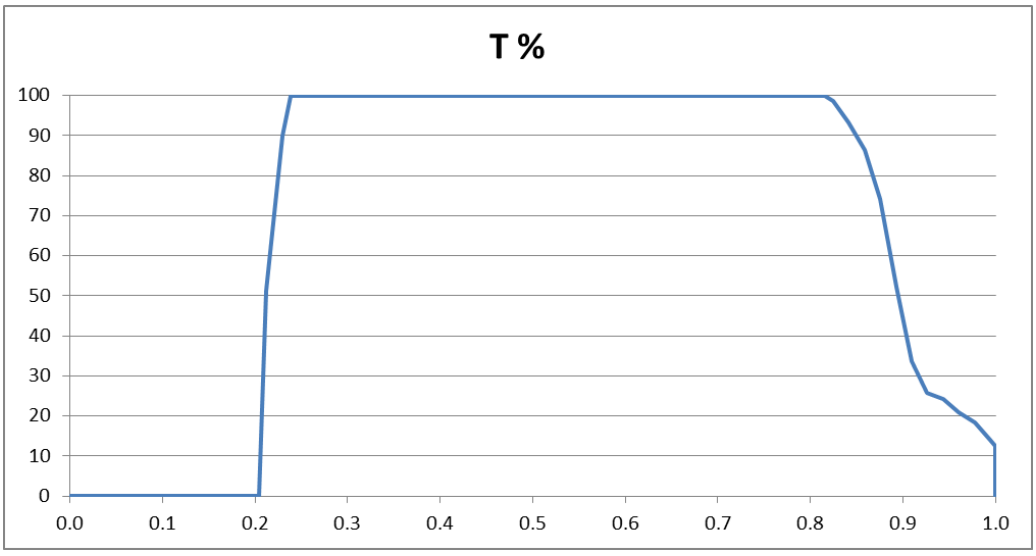

Figure 6. Average pupil transmission over all derotator angles. The horizontal axis is the normalized pupil radius.

To simplify the optical designing, an average pupil over all derotator angles was calculated. It gives a circular pupil with a variable transmission along its radius but the same in all directions (Figure 6). Such a pupil is much easier to handle and more precise than the average of the telescope pupil at a few derotator angles.

2.4 Final optical design

The present design has only 7 of the 23 slices but they are properly distributed to be representative. They are not weighted uniformly in the optimization process. The weight varies from 1 to 5 depending on how representative a slice is. Figure 7 shows the layout of the IFU. Top and side views are shown. The fore-optics are shown separately on the right for clarity. The fold bends the light at 90° toward the fore-optics which magnify the field; the magnification is a bit larger in the spectral direction.

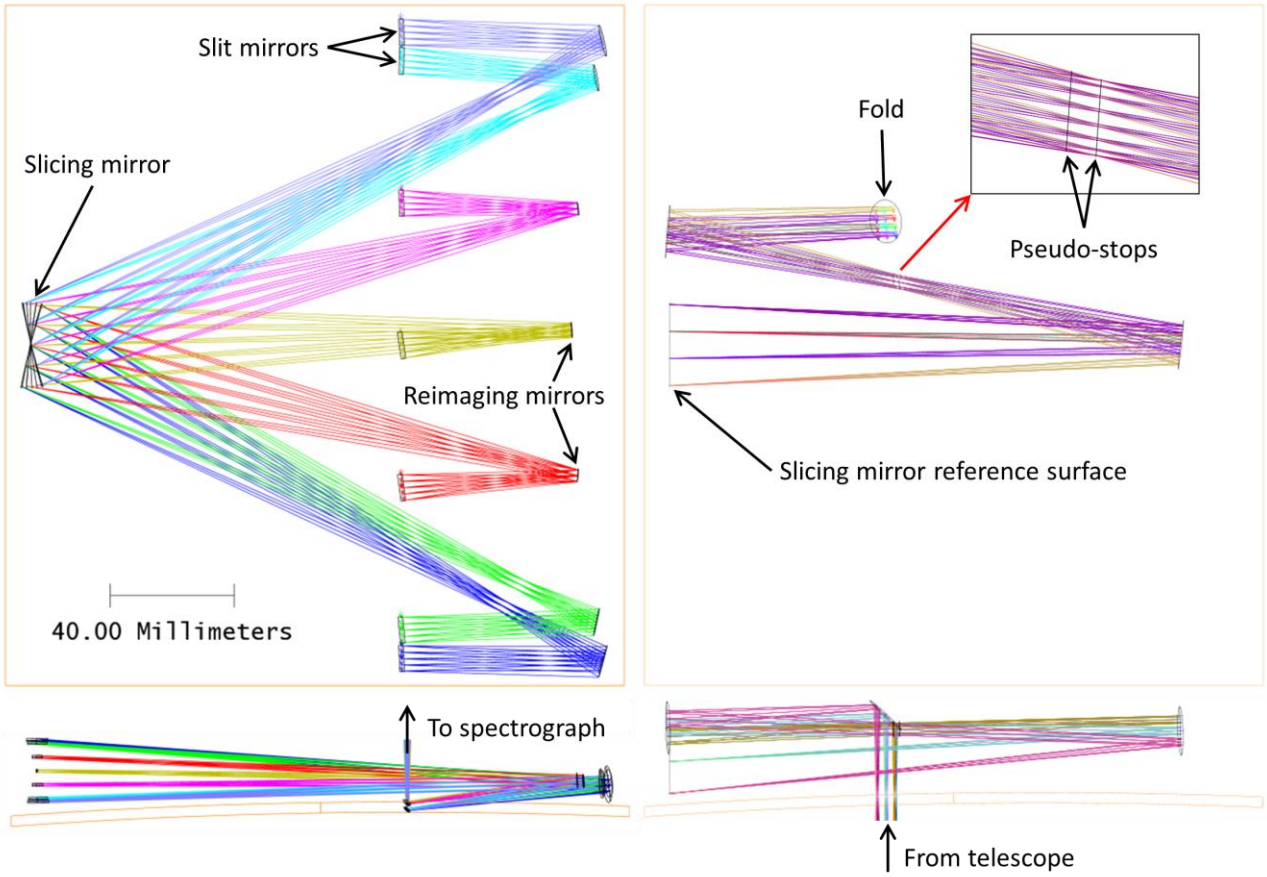

Figure 7. Layout of the IFU, top and side views are shown; the fore-optics are shown separately for clarity.

There is an intermediate pupil between the 2 fore-optics mirrors which are toroidal to accommodate the different magnifications along and perpendicular to the slices. The pupil then suffers from astigmatism but a stop there is very useful to cut any stray light and for alignment of the pupil. Instead of a stop, we use 2 baffles that we call pseudo-stops to solve the problem. One is in the vertical focus, the other the horizontal. In the out-of-focus direction, they are enlarged to avoid blocking the light. Together, they behave almost as a unique stop except for a small oversize in the diagonal directions. This solution was used successfully in the TAIPAN and Hector spectrographs [8] on the UK-Schmidt and the AAT telescopes. The left panel of Figure 7 shows the design from slices to slit mirrors. We can see that the reimaging mirrors are not sending beams perfectly parallel to each other on the slit mirrors. The reason is that the positions of the reimaging mirrors was optimized to maximize the image quality on the slit and pupil planes with the condition to have sufficient space between adjacent reimaging mirrors to avoid vignetting. The footprints of the beam on the missing mirrors were modelled to calculate the minimum distance needed between adjacent mirrors in the present design with

only 7 of them. Not seen in Figure 7 is the tilt along the slit of the beam leaving the slit mirrors toward the spectrograph, about 4°.

In the standard AIS design, the pupil images are on the reimaging mirrors or almost, so their name of pupil mirrors, but not in the present design. We can see the position of the pupil before the edge reimaging mirrors. The distance is quite large. This comes from the need to use a unique radius of curvature for all the slices to reduce cost. They can then be all polished at the same time. The larger distances between slice and reimaging mirrors at the edge leave the pupils before the reimaging mirrors while they are after them in the centre.

To reduce cost, there is a symmetry 2-by-2 of the reimaging and slit mirror surface forms. For example, the edge reimaging mirrors for slices 1 and 23 have the same toroidal surface shape. The same is true for reimagings mirrors for slices 2 and 22, and so on. The central mirror, for slice 12, is unique due to the odd number of slices. The same is true for the slit mirrors.

All reimaging mirrors are toroidal for 2 reasons. First, the large incident angle on the edge mirrors would create aberrations that are too large on the slit. Second, we want to modify their shape to correct some of the aberrations in the spectrograph, otherwise some in the centre could be spherical. Ideally, all the slit mirrors would also be toroidal but this would be too expensive for our budget so we settled for having only 8 out of 23, the 4 at the edge of the mirror line on each side which are the one that were generating the largest degradation of the pupil in the spectrograph.

2.5 Coatings

Standard reflections coatings as enhanced silver do not give a particularly good transmission in the region 360 nm to 420 nm. Dielectric coatings can theoretically give an excellent transmission over the whole range from 360 nm to 1000 nm but the needed precision is difficult to obtain since there are of the order of 1000 layers in these coatings. Errors generate absorption spikes in the transmission curve. To solve this problem, a first trade-off is made between average transmission and the risk of having these spikes. Since these coatings cannot be removed and remade, as opposed to silver coatings, the whole optics needs to be manufactured again if the coating is still not acceptable. We have 6 reflections along the optical train. Some of our optics, as the fold, fore-optics and spherical slit mirrors, are sufficiently low cost to be remanufactured but not the slicer. The toroidal mirrors are of intermediate cost but still expensive. There is then a second tradeoff to be made: the fold, fore-optics and slit mirrors will have a high performance dielectric coating while the slicer and probably the reimaging mirrors will have an enhanced silver coating. This should give us a transmission of at least 90% everywhere except at the shortest wavelengths where it should still be around 80%.

3. IMAGE QUALITY

3.1 Pupil image quality

The pupil image degradation remains however too large; there would be some vignetting on one of the grating that has a tight aperture in the spectral direction. The problem in not so much the loss of transmission which would be quite small but the variable loss due to the hexagonal shape of the telescope pupil combined with the rotation of the pupil with the telescope derotator (Figure 8). This would introduce systematic errors if calibration is done with a different pupil derotation angle than observing or if different observations are compared. To solve this problem, the pupil was reduced in the spectral direction by magnifying the slice images on the slit. By conservation of the A.Omega product, an increase in magnification by a factor of 1.125 in the spectral direction reduces the pupil by 1/1.125 in that direction. Figure 9 shows that the pupil now fits in its nominal diameter in the spectral direction (horizontal) while being still oversized in the spatial where the grating aperture is larger, so less critical. This would in principle reduce the resolution but the spectrograph was designed for a 0.6” slit which can accept larger aberrations, so they dominate the resolution with 0.305” slices. The reduction of pupil size reduces the spectrograph average PSF size. *The combination of larger slice images and smaller PSFs leaves an average resolution almost identical.*

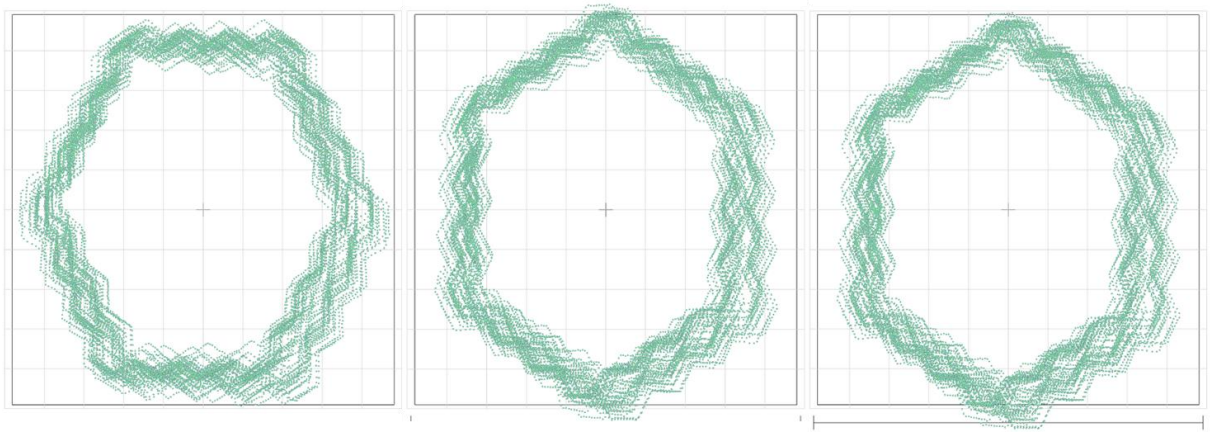

Figure 8. Pupil image on the grating with the tightest aperture in the spectral direction (vertical) at 30° rotation from each other (left and centre); with an additional decentering due to the IFU tolerances (right). Both spectrograph and slicer pupil aberrations are present.

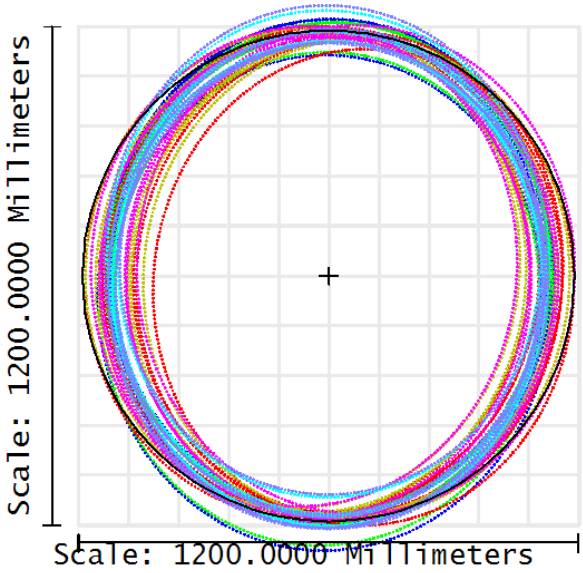

Figure 9. Output pupil of the slicer, the black circle shows the nominal pupil of the telescope which is almost identical to the maximum size of the secondary.

3.2 Field image quality

The final product of a slicer image on the detector is a 3-D data box in which we have an intensity as of function of (x, y, λ). There are then 3 one dimensional PSFs. The spatial PSF along the slice is the combination of all aberrations from telescope to detector. On the perpendicular direction, it is the PSF on the slicing mirror that matters; each slice is there like a spatial pixel. The spectral PSF is obtained on the detector from point sources on the slices because it is the edges of the slices that must be perfectly imaged. Figure 10 shows the PSF on the slicing mirror while Figure 11 shows the PSF on the slit for the worst slice from point sources on the slicing mirror. The spatial PSF along the slices is a combination of the two.

The image quality on the slicing mirror is excellent. The values are to be compared to a typical seeing of 0.6" which would be 1770 µm wide on the slicer. The image quality on the slit is still very good even for the worst slice although not negligible in the spectral direction. The spectrograph aberrations are typically much larger.

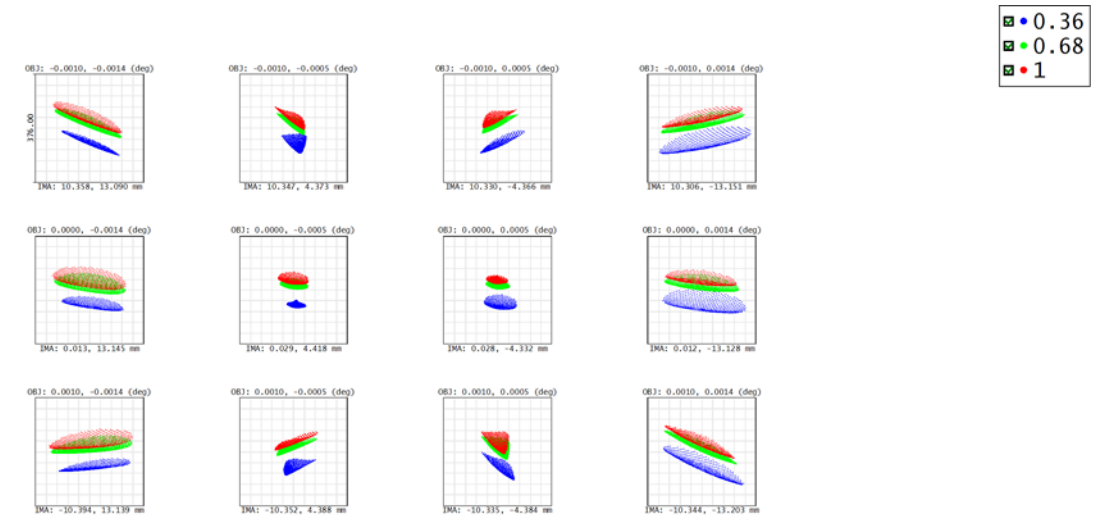

Surface IMA: Slicer

Spot Diagram

OSIRIS after lens manufactured, 15/07/2022
Units are µm. Legend items refer to Wavelengths

Field	1	2	3	4	5	6	7	8	9	10	11	12
RMS radius :	66.494	43.469	47.579	78.722	67.302	39.524	39.173	71.394	74.383	47.809	45.314	73.947
GEO radius :	150.029	97.392	104.722	171.186	137.508	71.234	87.702	167.691	157.791	105.926	113.873	182.875

Box width : 376 Reference : Centroid

Fore-optics MAAT dds120 pupcircor 10x7 slicp9 C01dbo.zos
Configuration 1 of 1

Figure 10. PSF on the slicing mirror, the boxes have the width of a pixel, so 0.127", in the horizontal direction, and the width of 1.125 pixel in the vertical. Spectral direction is horizontal.

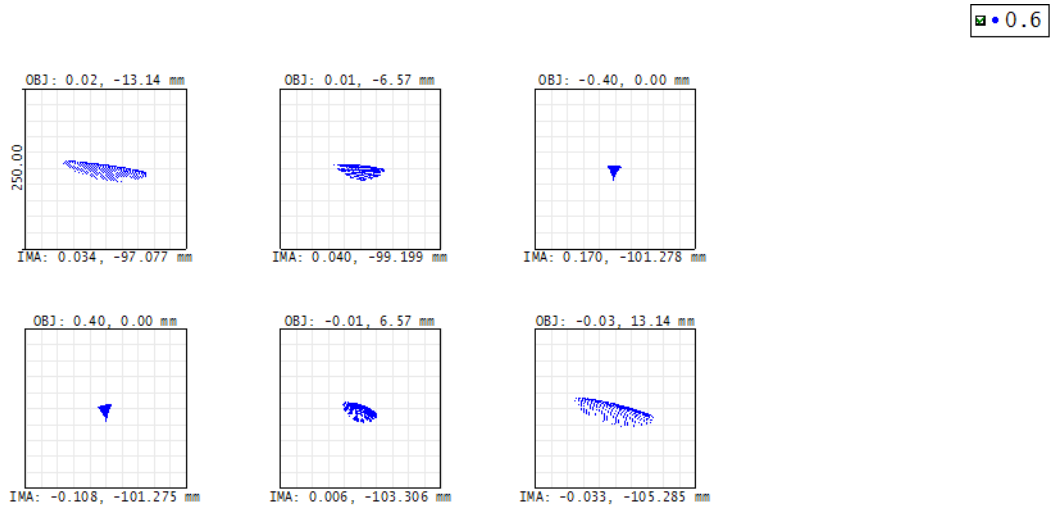

Surface 34: Slit mask apertr

Spot Diagram

MAAT slicer, 15/07/2022
Units are µm. Legend items refer to Wavelengths

Field	1	2	3	4	5	6
RMS radius :	31.964	19.081	6.615	7.194	13.763	30.507
GEO radius :	68.389	41.114	18.350	19.663	28.190	64.061

Box width : 250 Reference : Centroid

Figure 11. PSF of the worst slice on the slit, the boxes have the width of a slice image, so 0.305", in the horizontal direction, and the width of 1.125 slice images in the vertical. Spectral direction is horizontal.

3.3 Correcting some of the spectrograph aberrations

Compared to a standard slit of 0.6", the slices of 0.305" increase the spectral resolution. Assuming a Gaussian spectrograph PSF of 0.3" in width, a reasonable value for a 0.6" slit, spectral resolution would be 1.6 times higher with the slicer than with the standard slit. This adds to the fact that all the light of the objects will be captured except for the losses in transmission of the IFU then making it of great usefulness even for point sources. The increased resolution is however theoretical. The as-designed aberrations are known from the spectrograph optical design but this does not include the alignment aberrations which can easily dominates the PSF. Real measurements of the PSF on the detector must be done. We are in the process of measuring the PSF by using 2 out-of-focus masks with a series of pinholes along the slit. Each mask has its own frame to support it in the mask cartridge that permits to insert it in the spectrograph input focal plane. The masks have each 50 pinholes 0.2 mm in diameter at about 6.5 mm from each other and are positioned 30 mm before and after the telescope focal plane. The critical choice of the pinhole size is a trade-off between excessive blurring of the images if too large and excessive blurring of the pupil in the spectrograph due to diffraction focal ratio degradation if too small. The defocus was made as large as seems reasonably feasible. The pinholes give highly defocused images on the detector that encode the aberrations in the form of intensity and overall shape variations. With no aberrations, we would get an image that has the shape of the primary but affected by diffraction so depending on the wavelength(s) at that position on the detector (Figure 12). Astigmatism for example would reduce the defocus in one direction and increase it in the perpendicular direction which would change a circular image into an ellipse. Note that the shape of the GTC primary is far more complex than a simple circle and diffraction effect cannot be discarded but the information is there and can be dig out with the proper software. To confirm our calculations, we also took images of a mask with pinholes in the focal plane. Images were taken with the main gratings and in imaging with different arc lamps. In principle, we could have taken images with only one mask but there are advantages to have 2. First, we do not rely on the prefect knowledge of the mask position. Second, steep aberration curvatures on one image that makes the analysis difficult are not on the other because the curvatures of the wavefront due to the defocus are of opposite signs. In one image, the aberration curvature is increased while it is reduced in the other.

Figure 12. Out-of-focus images of a PSF with no aberrations using wave optics. The unusual shape is due to the shape of the GTC secondary mirror which is the stop of the telescope.

Figure 13 shows the image of a pinhole with both masks. The pinhole positions on each mask were chosen to give the same positions on the detector except for a small error due to the assumed position of the telescope pupil (tilt aberration). We can see that they are of very different sizes which show that the main aberration is defocus. This is not surprising because the focusing mechanism of OSIRIS was broken when these images were taken. It has been repaired when OSIRIS was moved from Nasmyth to Cassegrain focus.

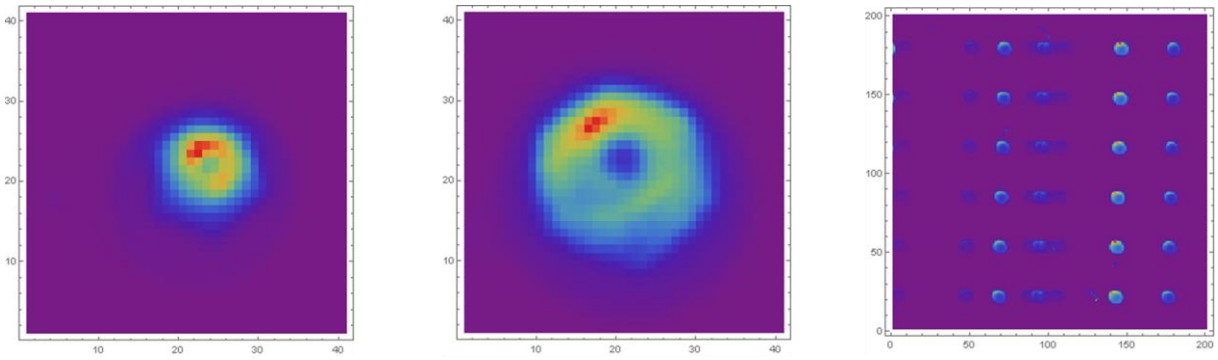

Figure 13. Out-of-focus images of a pinhole with the 2 out-of-focus masks (left & centre). Spectra of pinholes obtained with an arc lamp (right); spectral direction is horizontal.

Knowing these aberrations, modifications to the IFU can be made to correct at least some of them. This can be done because the real slit of the system is the set of slices on the slicing mirror. There is then additional optics in the "extended" spectrograph, especially the slicer system reimaging mirrors. Each of these mirrors reimages only a short slice image on the slit of the spectrograph so its aberrations do not vary much along that slice. Modifications to the reimaging mirrors can then correct the local spectrograph aberrations. Misalignments will mainly create defocus, coma, astigmatism and spherical aberration. Defocus and astigmatism can easily be corrected. Since the reimaging mirrors are toroidal, the correction is simply done by changing the surface form values given to the manufacturer. Coma and spherical aberration corrections would however mean making the reimaging mirror surface shapes more complex which would increase the cost. We will then only correct for local defocus and astigmatism. Tests done with Zemax in which it is the RMS of the PSF on the detector that is minimized instead of on the slit showed that it is effectively possible to do some spectrograph aberration corrections with the reimaging mirrors. The spectrograph slit then becomes an intermediate image that is not anymore of good image quality because of the inverse aberrations of the spectrograph there.

4. CONCLUSION

The work done shows that an image slicer can be added to the OSIRIS spectrograph without any show stopper. The IFU will considerably increase the throughput of the spectrograph compared to a 0.305" slit that would scan an object in the sky with 23 observations. Compared to a 0.6" slit, it increases the spectrograph resolution by probably a factor 1.6. To ensure this improvement, we have taken images with out-of-focus masks to measure the spectrograph aberrations and will correct as much as possible these aberrations by modifying the reimaging mirror shapes. The IFU design had a series of challenges as the maximum weight that the mask holder can support, the tilted and curved slit, the large incident angle on the reimaging and slit mirrors, and the low efficiency of standard reflective and anti-reflection coatings over the 360 nm and 1000 nm range but all were solved.

ACKNOWLEDGEMENTS

The work presented here would have been impossible without the technical support and help of the GTC staff. We thank IAA-CSIC (Granada, Spain), DARK (Copenhagen, Denmark), OKC (Stockholm, Sweden) and USAL (Salamanca, Spain) to provide the necessary funding for the Final Review Phase of MAAT that supports the work presented in this paper.

REFERENCES

[1] F. Henault, R. Bacon, R. Content, B. Lantz, F. Laurent, J.-P. Lemonnier & S. L. Morris, “Slicing the universe at affordable cost: the quest for the MUSE image slicer,” Proc. SPIE 5249, 134-145 (2004).

[2] P. J. McGregor et al, "Gemini near-infrared integral field spectrograph (NIFS)," Proc. SPIE 4841, 1581-1591 (2003).

[3] J. R. Allington-Smith, G. J. Murray, R. Content, G. N. Dodsworth, B. W. Miller, I. Jorgensen & I. Hook, “Integral field spectroscopy with the GEMINI multiobject spectrographs,” Exp. Astron., 13, 1-37 (2002).

[4] J. Schmoll, G. N. Dodsworth, J. R. Allington-Smith, R. Content, G. J. Murray & D. J. Robertson, “Design and construction of the IMACS-IFU, a 2000-element integral field unit,” Proc. SPIE 5492, 624-633 (2004).

[5] J. R. Allington-Smith, C. M. Dubbeldam, R. Content, C. J. Dunlop, D. J. Robertson, J. Elias, B. Rodgers & J. E. H. Turner, “An Image-Slicing Integral Field Unit for the Gemini Near-Infrared Spectrograph”, Proc. SPIE 5492, 701-710 (2004).

[6] R. Content, "Optical design of the KMOS slicer system," Proc. SPIE 6269, id. 62693S (2006).

[7] J. J. Bryant et al, "SAMI: a new multi-object IFS for the Anglo-Australian Telescope," Proc. SPIE 8446, 84460X (2012).

[8] J. Bryant et al, "Hector: a modular integral field spectrograph instrument for the Anglo-Australian Telescope," Proc. SPIE 10702, 107021H 7 (2018).

[9] R. Content, A. de Ugarte Postigo, C. Thöne & A. Sheinis, "The advanced image slicers of OCTOCAM," Proc. SPIE 10706, 107066L 9 (2018).

[10] R. Content, "Advanced Image Slicers for integral field spectroscopy with UKIRT and Gemini," Proc. SPIE 3354, 187-200 (1998).

[11] R. Content, "Advanced Image Slicers from the laboratory to NGST," Proc. ASP Conf. Series 195, 518-539 (2000).

[12] A. I. Sheinis, L. Laiterman, D. F. Hilyard & J. S. Miller, "Integral field unit for the echellette spectrograph and imager at Keck II," Proc. SPIE 4841, 1078-1085 (2003).

[13] C. M. Dubbeldam, D. J. Robertson, D. A. Ryder & R. M. Sharples, "Prototyping of diamond machined optics for the KMOS and JWST NIRSpec integral field units," Proc. SPIE, 6273, 62733F (2006).

[14] G. S. Wright et al, "Design and development of MIRI, the mid-IR instrument for JWST," SPIE, 7010, 70100T (2008).

[15] F. Prada, R. Content et al, "White paper on MAAT@GTC," arXiv, 2007.01603 (2020).

[16] R. Haynes, R. Content, J. Turner, J. R. Allington-Smith & D. Lee, "SMIRFS-II: multiobject and integral-field near-IR spectroscopy at UKIRT," SPIE, 3354, 419-430 (1998).